

Effects of cutting angle, edge preparation, and nano-structured coating on milling performance of a gamma titanium aluminide

Original

Effects of cutting angle, edge preparation, and nano-structured coating on milling performance of a gamma titanium aluminide / Priarone, PAOLO CLAUDIO; Stefania, Rizzuti; Settineri, Luca; Guido, Vergnano. - In: JOURNAL OF MATERIALS PROCESSING TECHNOLOGY. - ISSN 0924-0136. - STAMPA. - 212:(2012), pp. 2619-2628. [10.1016/j.jmatprotec.2012.07.021]

Availability:

This version is available at: 11583/2503396 since:

Publisher:

Elsevier

Published

DOI:10.1016/j.jmatprotec.2012.07.021

Terms of use:

This article is made available under terms and conditions as specified in the corresponding bibliographic description in the repository

Publisher copyright

(Article begins on next page)

Effects of cutting angle, edge preparation, and nano-structured coating on milling performance of a gamma titanium aluminide

Paolo Claudio Priarone ^{1*}, Stefania Rizzuti ¹, Luca Settineri ¹ and Guido Vergnano ²

¹ Department of Management and Production Engineering,
Corso Duca degli Abruzzi 24, 10129 Torino, Italy

² Fratelli Vergnano S.r.l., Corso Egidio Olia 2, 10023 Chieri, Torino, Italy

* Corresponding Author

Phone: +39 011 0907206

Fax: +39 011 0907299

Email: paoloclaudio.priarone@polito.it

Abstract

Gamma titanium aluminides are intermetallic alloys. Recently, they have been evaluated as important contenders for structural applications in the automotive and aerospace sectors. This is due to their excellent high-temperature performances and their significantly lower density compared to Nickel-based superalloys. In this paper, an analysis of machinability of a gamma TiAl obtained via an electron beam melting (EBM) process is presented. The effects of tool geometry modifications, in terms of cutting tool angles and cutting edge preparation, were investigated. The reduction of radial rake angle and the drag finishing process for cutting edge preparation resulted in an increase of the tool life of the carbide end mills. Nanogradient tool coatings were also observed to affect tool wear during milling tests, and the results highlight that AlSiTiN coating performs better compared to CrAlSiN coating. A post-coating polishing treatment was also taken into account, and it allowed a further reduction of tool wear. The overall results indicate that the machinability of this difficult-to-cut material can be significantly improved by an adjustment of the cutting edge geometry, and by using an AlSiTiN coating system.

Keywords: Gamma titanium aluminide, EBM, nanostructured composite coating, cutting edge treatment, tool wear.

1. Introduction

Gamma titanium aluminides received much attention in recent years due to their attractive combination of properties, which offer a growing number of applications in the aerospace and automotive fields. These intermetallic alloys show low density, high strength/weight ratio, high temperature strength, fatigue resistance, and good oxidation resistance. At the same time, they are referred to as difficult-to-cut materials because of their high hardness and brittleness, low thermal conductivity, high chemical reactivity, and a strong tendency to hardening.

Over the past few decades, the effects of the composition, preparing method, and microstructure on the mechanical behaviour of TiAl alloys have been widely investigated, as reported by Liu and Maziasz (1998) and Liu et al. (2002). While studies on their machinability with conventional and unconventional processes still require an in-depth analysis, as pointed out by Aspinwall et al. (2005), a limited number of publications which have focused on conventional machining processes such as milling, turning, and drilling can be found in the scientific literature. Furthermore, the obtained results are strongly dependant on the specific alloys and on their employed production technology.

As far as milling of gamma-TiAl is concerned, Mantle and Aspinwall (2001) investigated the surface integrity of a high speed ball end milled gamma titanium aluminide Ti-45Al-2Nb-2Mn-0.8 vol. % TiB₂ XD, that was induction skull melted, investment casted, HIPed, and heat treated. The tests were conducted with coated tungsten carbide ball end tools, and with operating parameters of finishing machining. Workpiece surface alterations included material pullout, fracture, smearing, and

deformation of the lamellae. The surface roughness values measured were low, and the surface contained compressive stresses. In addition, tool flank wear and cutting speed were found to have the greatest effect on residual stress.

Beranoagirre and López de Lacalle (2010) presented the results of milling tests on three different types of gamma TiAl alloys: the MoCuSi type in ingot and extruded form, and the TNB type in ingot form. They analysed the flank wear as a function of cutting time for different cutting conditions, and found that the cutting speed has the main effect on the tool life of hard metal end milling tools.

Recently, Priarone et al. (2011) investigated the machinability in milling of a gamma titanium aluminide, fabricated via electron beam melting and then thermally treated. Electron beam melting (EBM) is a direct-metal freeform fabrication process in which an electron beam with a constant acceleration voltage is used to selectively densify metal powder in a layerwise manner to produce high density near net shape components. This study highlighted that the machinability of this EBM sintered γ -TiAl alloy is strongly influenced by process parameters and lubrication conditions (dry, wet, and minimum quantity lubrication were tested), as far as tool wear and surface quality are concerned.

Nevertheless, there remains a need to improve the machinability of these difficult-to-cut alloys, in order to increase the use of this promising material in the aerospace market. An encouraging strategy was identified by the authors in tool optimization, in terms of cutting tool angles, cutting edge treatments, and by applying super hard and high toughness nanocomposite coatings. This paper focuses on two fundamental aspects related to the machinability of an EBM sintered γ -TiAl alloy: firstly, the influence of tool geometry and of the edge treatments is investigated, and secondly, the effect of the deposition of tool coatings on the carbide mills is explored. All these influencing factors are analyzed with respect to tool wear, surface roughness and hardness, and machined chip.

2. Experimental tests

2.1. Experimental set-up and procedures

A set of experimental tests was carried out in order to investigate the effects of tool geometry modifications and coatings on the machinability of a gamma-TiAl alloy. All the milling tests were performed on a Ti-48Al-2Cr-2Nb (atomic %) EBM sintered γ -TiAl alloy, with the chemical composition detailed in Table 1. The EBM process starts from metal powders, and melts them, layer by layer, with an electron beam in a high vacuum. This allows the manufacture of parts in reactive materials, such as titanium, with a high affinity for oxygen (Cormier et al., 2007). The process is usually followed by heat treatment. The sample used for these tests was a block measuring 120 x 120 x 30 mm, subjected to 5 hours at 1095 °C, hot isostatic pressing for 4 hours at 1285 °C, then 2 hours at 1305 °C. The employed gamma-TiAl alloy, as provided by the material supplier, showed a tensile strength equal to 345 MPa, a yield strength (0.2% offset) of 276 MPa, and an elongation (percent in 4D) equal to 0.5. In addition, the measured average initial hardness was 273 HV₃₀, with a standard deviation of 5.2 HV₃₀.

Element	Weight percent
Aluminum	32.0 - 33.5
Niobium	4.5 - 5.1
Chromium	2.2 - 2.6
Oxygen	Max 0.08
Nitrogen	Max 0.02
Carbon	Max 0.015
Iron	Max 0.04
Hydrogen	Max 0.001
All others	Max 0.05
Titanium	Balance (Max 60%)

Table 1: Chemical composition of EBM sintered γ -TiAl alloy.

The additive manufacturing process used to obtain the workpiece material is suitable to obtain freeform near-net-shape parts, and it is successfully used for various applications, such as components for biomedical implants, as reported by Murr et al. (2009). However, as shown in Figure 1, the surface quality achieved by an EBM process is not adequate to meet the strict requirements of the aerospace and automotive industry, therefore further finishing or semi-finishing machining operations are needed.



Figure 1: EBM sintered workpiece, as supplied.

In order to perform microstructural observations, some samples were randomly extracted from the workpiece, ground, polished, and then etched in a Keller solution. The analyses were performed by using an inverted optical microscope Leica MEF4U, and revealed a lamellar microstructure with a different orientation of the lamellae and some porosity (Figure 2). It is important to note that, the EBM process does not deliver a material completely void-free (Petropoulos et al., 2010; Cotterell and Byrne, 2008), and in the present case, the density was estimated to be around 98%. In order to prepare the workpiece for the experimental tests, a preliminary flat-grinding operation was performed (Figure 3).

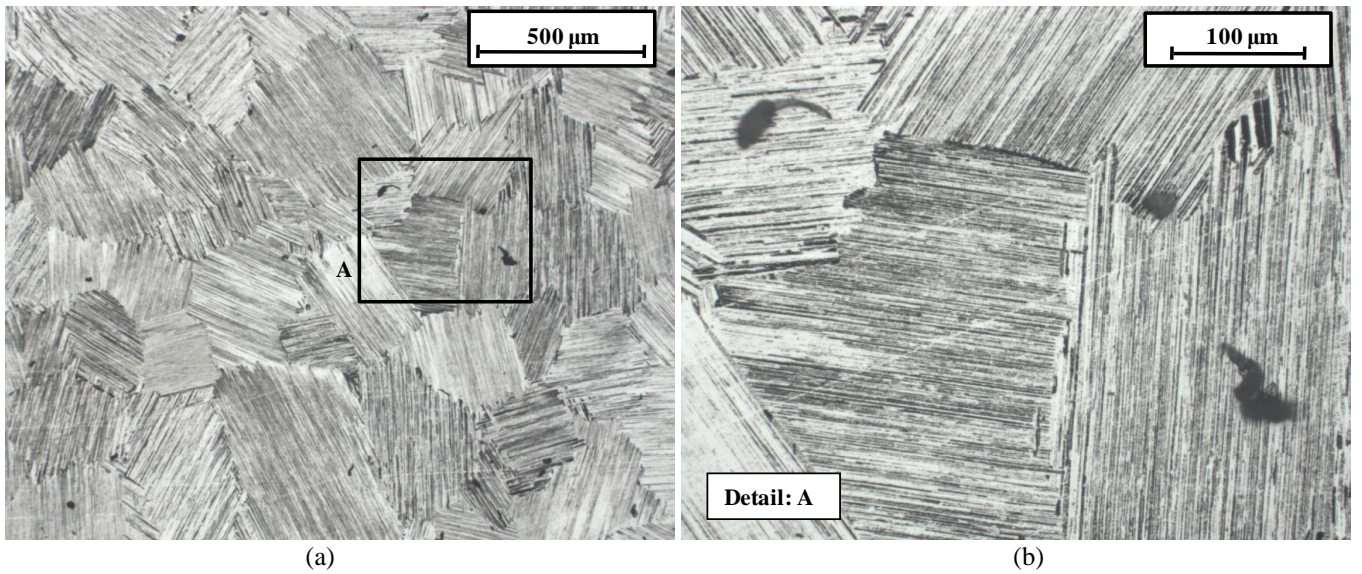


Figure 2: Workpiece microstructure, at different magnifications: 50X (a) and 200X (b).

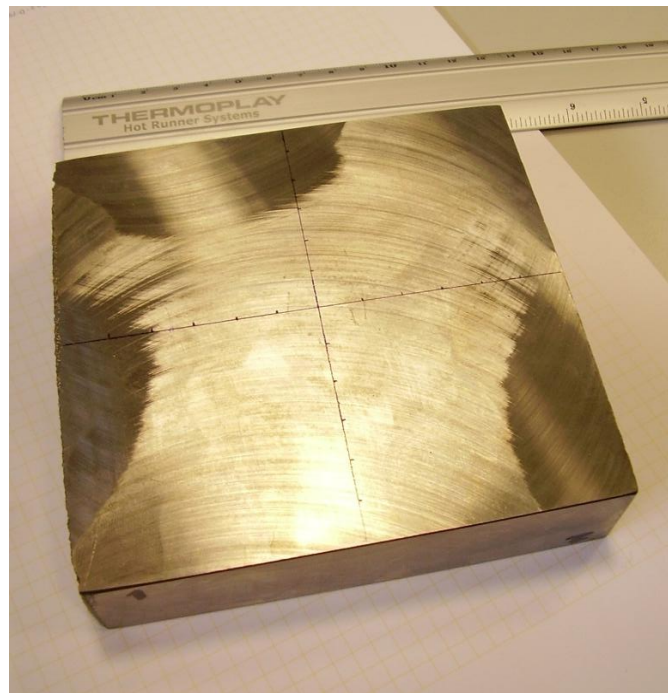


Figure 3: Workpiece grinded prior to milling operations.

Milling tests were executed by means of a three axis Cortini M500/F1 vertical CNC milling machine, characterized by a continuously variable spindle that reaches up to 8000 rpm, with a peak power of 3.7 kW and a maximum torque of 24 Nm. Earlier research activities showed that, cutting performances with uncoated carbide mills are affected by process parameters and lubrication conditions (Priarone et al., 2011). Moreover, tool life prolongation can be obtained by reducing feed per tooth and cutting speed, and by using a minimum quantity lubrication system. The focus of this work is tool optimization, and with reference to the same range of process parameters formerly adopted, cutting conditions were fixed as follows:

- cutting speed: $v_c = 50$ m/min;
- feed per tooth: $f = 0.10$ mm/tooth;

- axial depth of cut: $d_z = 0.3$ mm;
- radial depth of cut: $d_r = 0.3$ mm.

All the milling operations were performed in dry lubrication conditions, and in a down-milling direction. Tool overhang length was 30 mm. Tool wear was periodically measured at different cutting times, by means of a stereo microscope Leica MS5 (with 40X magnification) equipped with a high resolution camera Leica DFC280 for image acquisition. Tool observations were also performed using a scanning electron microscope LEO 1450 VP with a tungsten filament, equipped with an EDS microprobe for elemental analysis, and a secondary electron and backscattered detectors for image collection. The arithmetic mean roughness value R_a , the maximum roughness profile height R_t , the skewness R_{sk} , and the kurtosis roughness R_{ku} were measured in the feed direction by a Hommelwerke Tester T1000. The instrument's accuracy corresponds to DIN 4772 Class 1, and the resolution is equal to $0.01 \mu\text{m}$ with the measuring range of $\pm 80 \mu\text{m}$. The generated surface hardness was measured by a Emcotest M4U 025 universal hardness tester, adopting the HV_{30} test conditions (load of 30 kg applied with a pyramidal indenter for 30 s). For this Vickers test, the machine's calibration certificate identifies a maximum measurement error of 0.34%. Observations of the generated surface were performed using an inverted optical microscope Leica MEF4U, while chip morphology was also investigated by SEM.

2.2. Tool geometries

As mentioned, the first part of this experimental research focused on the investigation of the effects of tool geometry modifications on the alloy machinability. Vergnano 10-mm diameter ISO K30/K40 carbide end mills with 4 uncoated edges were used. They are produced by a Walter Helitronic Vision 5-axis CNC grinding machine: Table 2 summarizes the geometrical parameters. Tools with different radial rake angles ($\gamma = 12^\circ$ and 4°) were employed, as shown in Figure 4.

Parameter	Value
Mill diameter (mm)	10
Shank diameter (mm)	10
Length of cut (mm)	23
Overall length (mm)	72
Axial rake angle ($^\circ$)	4
Axial primary relief angle ($^\circ$)	6
Axial secondary clearance angle ($^\circ$)	16
End cutting edge concavity angle ($^\circ$)	2
Helix angle ($^\circ$)	30
Radial rake angle ($^\circ$)	12; 4
Radial primary relief angle ($^\circ$)	12
Radial secondary clearance angle ($^\circ$)	12

Table 2: End mills geometrical parameters.

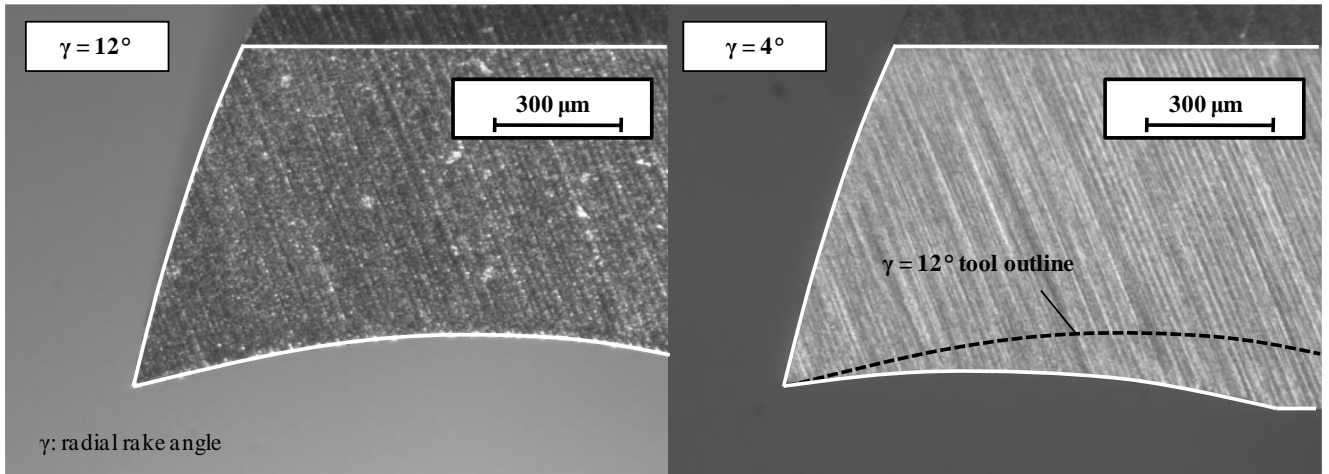


Figure 4: Fresh tool geometry comparisons.

The results obtained with sharp/as-ground mills were then compared with those achieved with tools subjected to a drag finishing treatment, performed on an Otec DF 70 machine. Figure 5 shows the rotating holding carousel fitted with five revolving spindles, which plunge the tools into a stationary medium. In the present case a nutshell granulate with SiC polishing powder mixture was adopted (trade name: HSC 1/300). Each tool describes a planetary motion and, at the same time, rotates on its own axis. In order to ensure a uniform rounding of the edges, the sense of rotation was periodically inverted during the process.



Figure 5: OTEC DF 70 drag finishing machine.

The radius of edge roundness r_β and the edge roughness R_{af} were measured at fixed time intervals, by means of an Alicona Infinite Focus microscope. As expected, the drag finishing process, exerting an abrasive action, increases the edge radius and

improves the edge surface quality: the roughness peaks are partially reshaped and thereby levelled. Both phenomena occur in the first minutes of the process, then the values settle around asymptotic values. Table 3 summarizes the geometric characteristics of the tools used in the cutting tests.

Test	Radial rake angle $\gamma(^{\circ})$	Edge treatment	Radius of edge roundness $r_{\text{p}}(\mu\text{m})$	Average edge roughness $R_{\text{a}}(\mu\text{m})$
1	12	None	≈ 5	0.64
2	12	Drag finishing	≈ 10	0.49
3	4	None	≈ 5	0.40
4	4	Drag finishing	≈ 10	0.23

Table 3: Uncoated tools for cutting tests.

2.3. Tool coatings

The second part of the experimental plan was designed to assess the potential benefits resulting from the use of coated tools. At the end of the first experimental phase, experimental PVD AlSiTiN and CrAlSiN nanogradient coatings were deposited onto the mills which had provided the best performances. The tool with the radial rake angle $\gamma = 4^{\circ}$ subjected to the drag finishing process was chosen. At this stage, the tool immersion depth in the medium (measured from the tool tip) was augmented from 45 mm to 130 mm: the increased pressure exerted by the abrasive medium enlarged the radius of edge roundness to $\approx 15 \mu\text{m}$, with an average edge roughness of $0.2 \mu\text{m}$.

The Physical Vapour Deposition (PVD) unit used to deposit the coatings was a Platit PL55 PVD LARC (Lateral Arc Rotating Cathodes), equipped with two cathodes: one made of titanium or chromium, and the second one made of Al-Si eutectic alloy.

Coating architecture, as shown in Figure 6, was designed as follows:

- an adhesion layer, composed of Ti(or Cr)N;
- a Ti(or Cr)AlSiN nanolayer with a period $< 20 \text{ nm}$;
- a Ti(or Cr)AlSiN gradient layer.

The coating distribution was made in order to achieve a constant thickness of approximately $3 \mu\text{m}$.

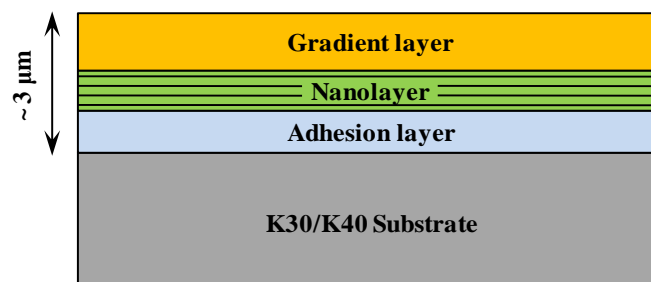


Figure 6: Structure of the experimental gradient coatings.

Finally, after the coating process, some mills were subjected to a further polishing post-treatment by using the HSC 1/300 stationary medium, in order to remove the droplets and to polish the tool without modifying the tool edge geometry. Table 4 details the coated tools used in the second part of the experimental plan.

Test	Radial rake angle γ (°)	Edge pre-treatment (before coating)	Radius of edge roundness r_β (μm)	Average edge roughness $R_{a\beta}$ (μm)	Coating	Edge post-treatment (after coating)
5	4	Drag finishing	≈ 15	0.20	AlSiTiN	None
6					AlSiTiN	Polishing
7					CrAlSiN	None
8					CrAlSiN	Polishing

Table 4: Coated tools for cutting tests.

3. Results and Discussion

The machinability of the EBM sintered γ -TiAl alloy was analysed in terms of tool wear, surface quality, and chip morphology. The obtained results are presented and discussed below.

3.1. Tool wear

The observation of tools during the milling process showed that wear mainly affects the cutting edge tip, and that corner wear is always more pronounced than flank wear (Figure 7). This result is common to all the tests performed at fixed process parameters ($v_c=50$ m/min, $f = 0.1$ mm/tooth, $d_z = d_r = 0.3$ mm), with both uncoated and coated tools. For instance, Figure 8 presents SEM 500X magnified images of a worn AlSiTiN coated and polished mill, after 40 minutes of cutting time: the micro-chipping of the cutting edge tip is clearly evident. Additionally, the presence of workpiece material adhering to the tool, as highlighted by the EDS analysis (Figure 9), was detected on all tools, particularly on the rake face.

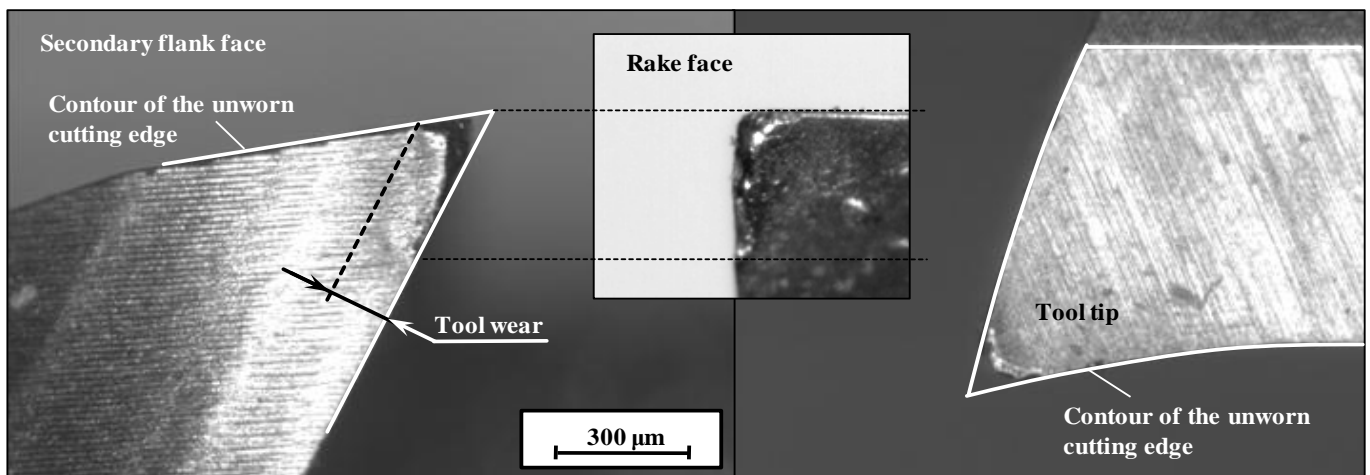
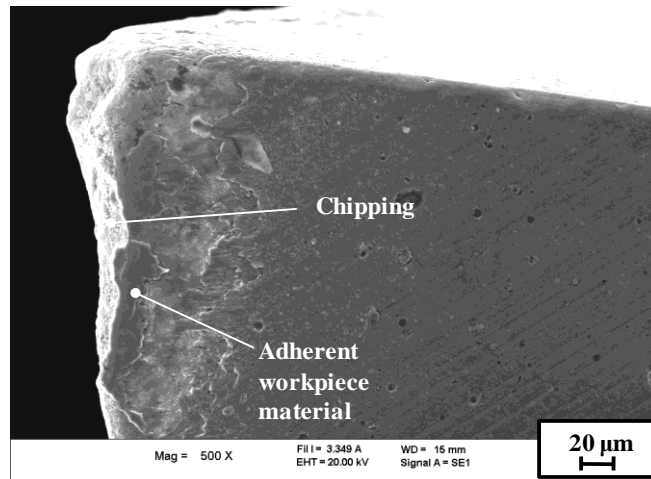
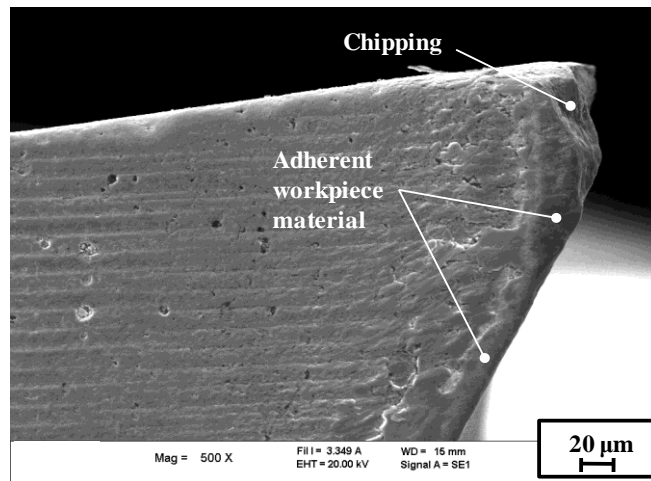


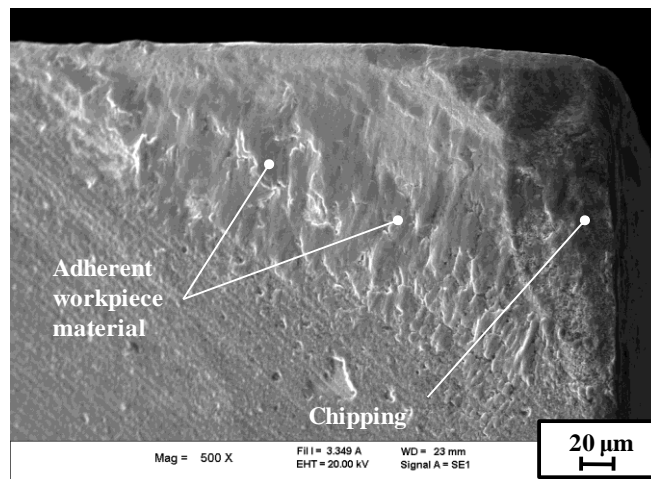
Figure 7: Tool wear observations. The images refer to an uncoated mill with radial rake angle $\gamma = 12^\circ$, without drag finishing treatment, and after 16 minutes of machining time.



(a)



(b)



(c)

Figure 8: SEM images of an AlSiTiN coated edge after 40 min of milling time: tool tip (a), secondary flank face (b), and rake face (c).

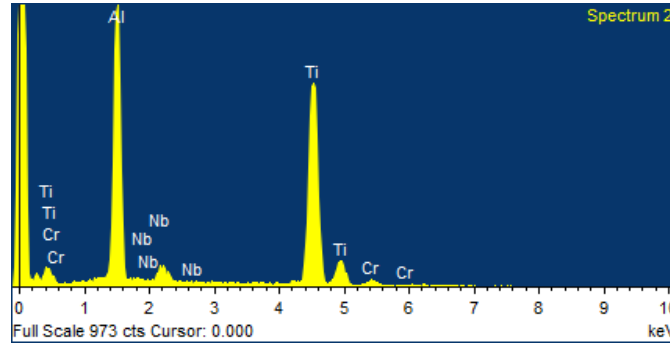


Figure 9: EDS analysis of adherent workpiece material.

The criterion used to quantify tool wear as a function of milling time is the maximum value between the flank wear and the corner wear measured on the secondary flank surface, as illustrated in Figure 7. Figure 10 shows the tool wear curves. Each point on the graphs corresponds to the average value of the measurements executed on the four edges of the mill. The tool wear limit was fixed at 100 μm , a restrictive condition usually adopted in finishing operations for aerospace and automotive components.

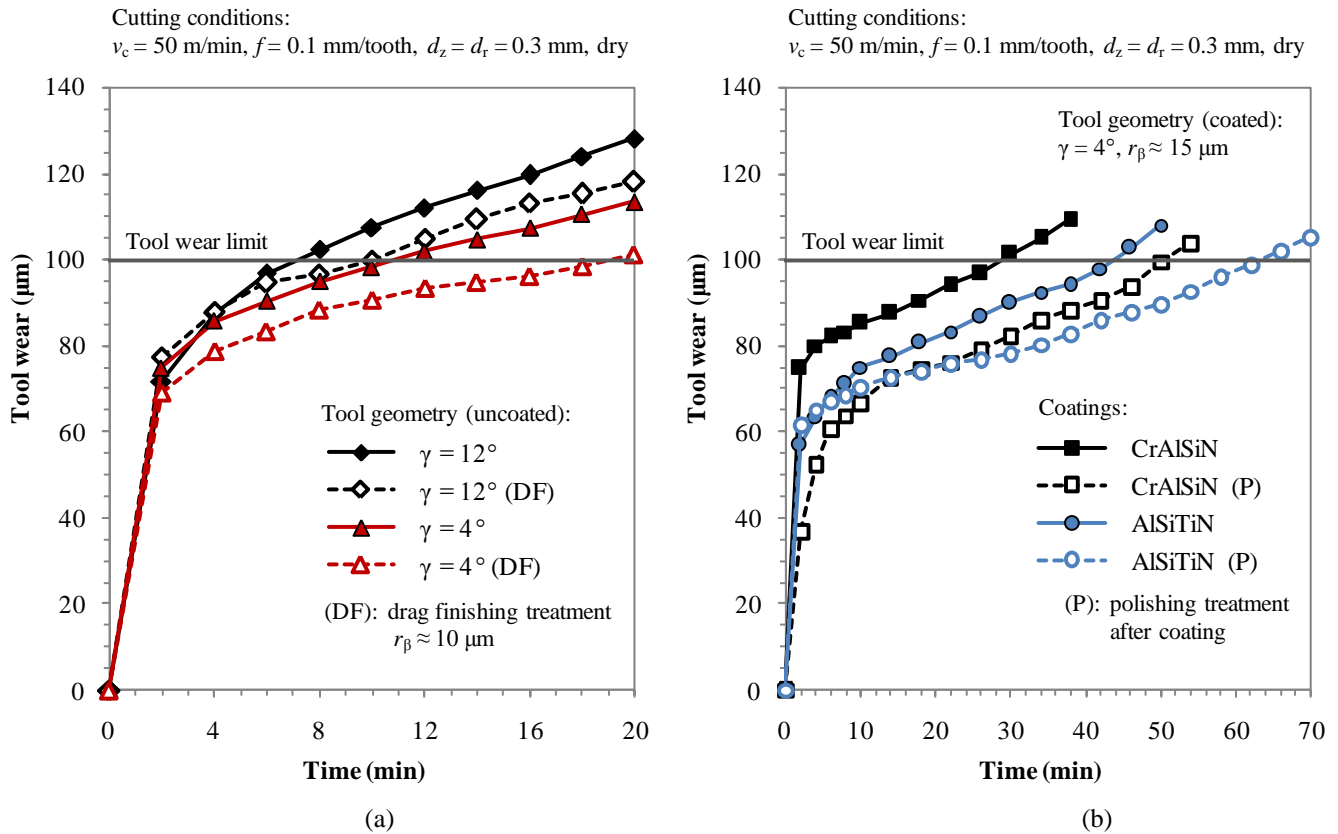


Figure 10: Experimental tool wear curves, for uncoated (a) and coated tools (b).

For uncoated carbide tools (Figure 10 a), the reduction of radial rake angle from $\gamma = 12^\circ$ to $\gamma = 4^\circ$ results in a benefit in terms of tool life, which is raised from 7.2 to 10.9 minutes. In addition, for both mill geometries, the drag finishing process makes it possible to increase tool life approximately by 40% for $\gamma = 12^\circ$ ($T_L = 10 \text{ min}$), and by 75% for $\gamma = 4^\circ$ ($T_L = 19.2 \text{ min}$). This is

due to the fact that the drag finishing process rounds the cutting edges and smooths the tool surfaces; consequently edge chipping and friction are reduced, and as a result tool wear decreases significantly.

The results of cutting tests executed with nanogradient coatings which were deposited onto mills with $\gamma = 4^\circ$ and $r_\beta \approx 15 \mu\text{m}$, highlight that AlSiTiN coating performed better than CrAlSiN coating, as shown in Figure 10 b: the resulting tool life was $T_L = 43.8 \text{ min}$ and $T_L = 28.8 \text{ min}$, respectively. This occurrence is also in agreement with the results obtained by Settineri et al. (2008) in dry milling operations of AISI M2 difficult-to-cut die steel, performed with tungsten carbide mills coated with similar nanostructured architectures. A second consideration is that the polishing treatment after coating permitted a further reduction in tool wear; the best result of $T_L = 63.6 \text{ min}$ was accomplished with Ti-based coating. As expected, droplet removal and the polishing of the coated surfaces improved the performance of the tools during the material removal process.

3.2. Surface roughness

Figure 11 presents the results obtained in terms of arithmetic mean roughness R_a and of maximum roughness profile height R_t , with reference to estimated tool life T_L , and for each test of the experimental campaign. The values that are reported in the histogram are the average values of the roughness indexes measured until the tool wear limit was reached, while the range bars specify the maximum and minimum values.

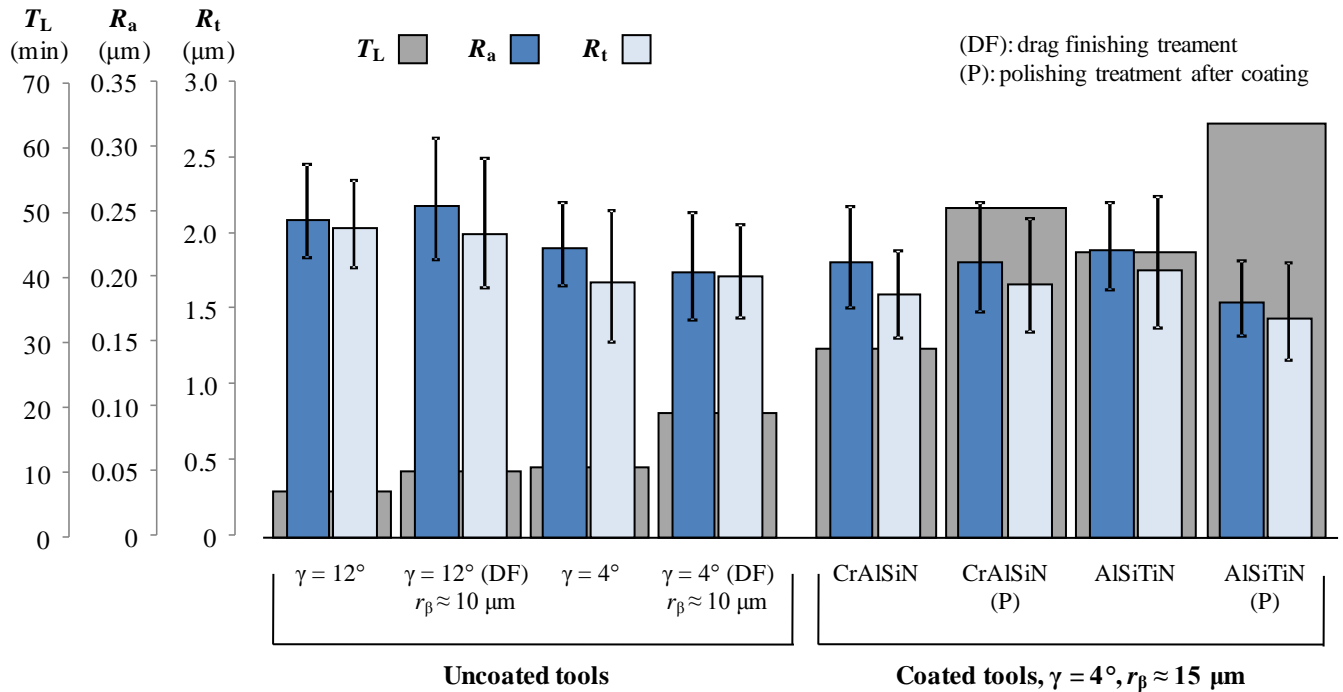


Figure 11: Roughness results.

For all the experimental tests R_a was less than $0.3 \mu\text{m}$, and R_t always had values below $2.5 \mu\text{m}$. Therefore, these parameters for surface roughness are suitable to satisfy demand for security for parts in aircraft engines ($R_a \leq 0.4 \mu\text{m}$, as suggested by Klocke

et al., 2008). Variations of average values of R_a and R_t are small but noticeable, and for the uncoated tools the radial rake angle $\gamma = 4^\circ$ yields better outcomes, while the drag finishing process does not involve considerable result changes. For the chosen cutting parameters, by far the best result was obtained by the mills which had AlSiTiN coating, and were subjected to polishing post-treatment: values of R_a and R_t equal to $0.18 \mu\text{m}$ and $1.43 \mu\text{m}$ were achieved, respectively. Those mills also had the longest tool life $T_L = 63.6 \text{ min}$, at a tool wear limit of $100 \mu\text{m}$. Lastly, no statistically significant variations for R_{sk} and R_{ku} indexes were detected on varying the type of tool/coating. The average values of R_{ku} were above 3 for all the tests ($3.1 < R_{ku} < 3.4$), while the R_{sk} measurements oscillated at around 0, with slightly negative mean values within the range of $-0.13 < R_{sk} < -0.02$.

3.3. Surface hardness

The graphs in Figure 12 and Figure 13 illustrate the results obtained in terms of HV_{30} surface hardness as a function of tool wear. Each point represents the mean value of three experimental hardness measurements, while the straight lines represent the linear interpolation of the data. The trends show that, from the initial average hardness measured on the workpiece of 273 HV_{30} , the milled surface hardness increases proportionally with tool wear, as a result of strain hardening.

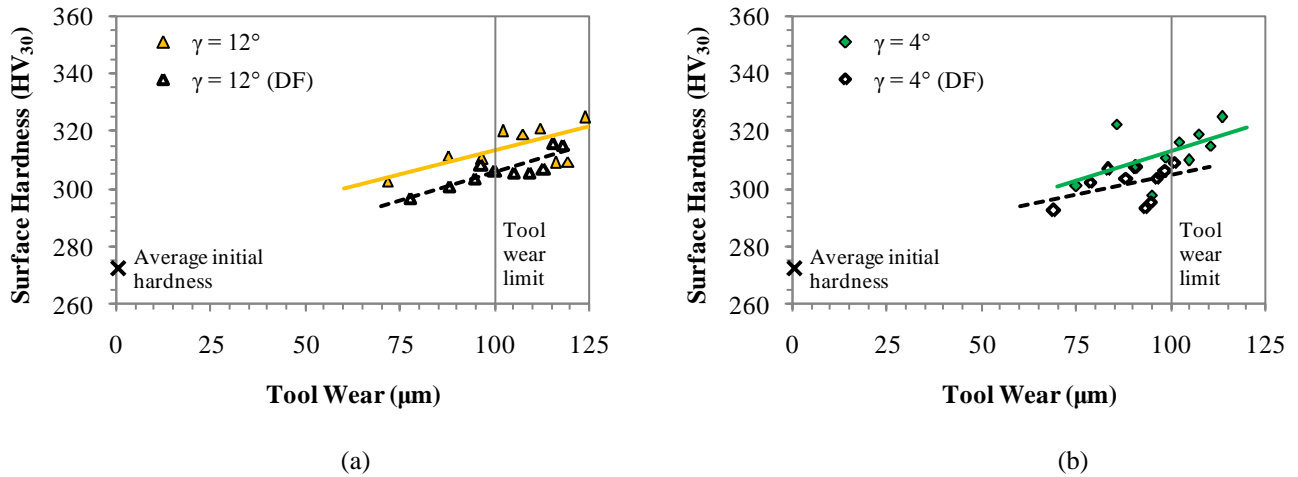


Figure 12: Surface hardness results for uncoated tools with radial rake angle $\gamma = 12^\circ$ (a) and $\gamma = 4^\circ$ (b).

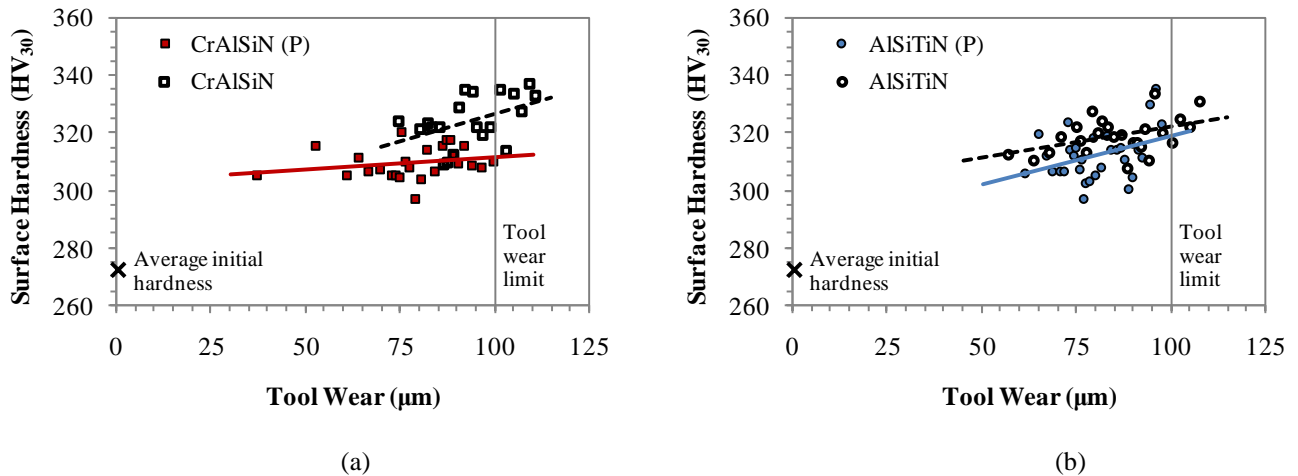


Figure 13: Surface hardness results for CrAlSiN (a) and AlSiTiN (b) nanocoated tools. Tool geometry is $\gamma = 4^\circ$ and $r_\beta \approx 15 \mu\text{m}$.

For uncoated carbide tools (Figure 12), no considerable result variations with the decrease of radial rake angle were detected, while for the same tool wear, the drag finishing process involves a moderate diminution of surface hardness. This occurs because of friction reduction due to better surface finishing on the cutting edges, which prevails on the effect of work hardening due to the increase of edge roundness.

Similar considerations can be applied to polishing treatment after coating (Figure 13): the improved surface quality of the polished cutting tool edges slightly reduces the surface hardness. Finally, on average, the hardness measurements of the surfaces milled with coated tools are higher than those obtained with uncoated mills. This occurrence is due to the abovementioned radius of edge roundness which increases from $\approx 10 \mu\text{m}$ to $\approx 15 \mu\text{m}$.

3.4. Surface structure

Observation by optical microscope of the milled surfaces showed the presence of micro-craters, due to the microstructure of the workpiece (Figure 2), which was produced from metal powders by means of a rapid manufacturing process (Yu, 2001). These outcomes are common both for coated tools, as evidenced in Figure 14, and for uncoated carbide tools, even with different process parameters, as found by Priarone et al. (2011).

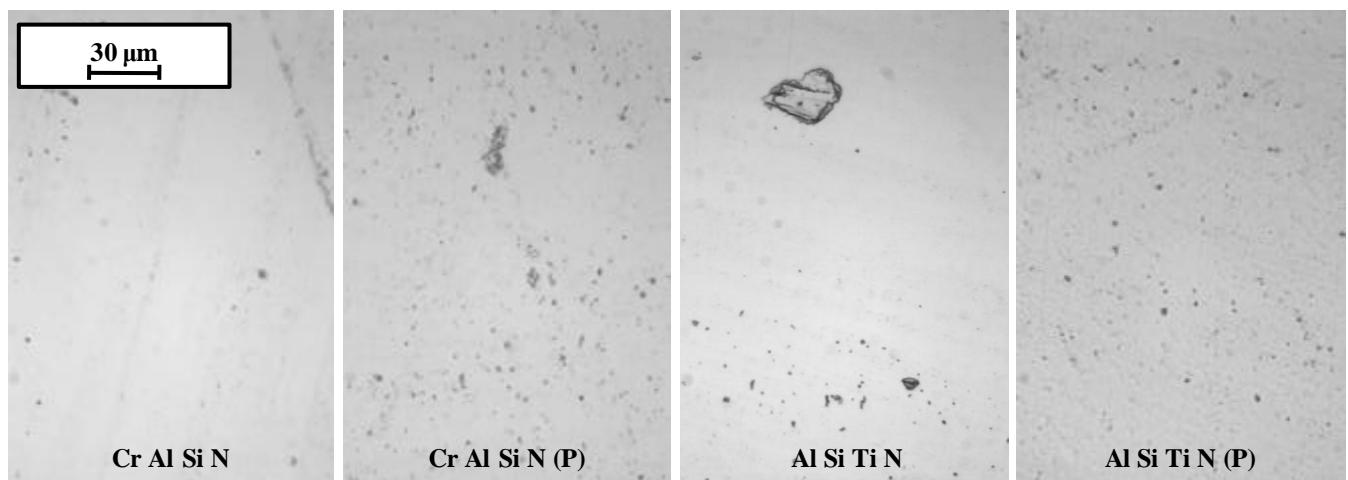


Figure 14: Micrograph of the milled surface (500X) for different coated tools.

3.5. Chip morphology

In each test, machined chips were collected and imaged in the SEM. Chips presented a shear-localized form, as for other difficult-to-cut materials, such as titanium alloys, nickel-based superalloys, hardened alloy steels, and stainless steels (Hou and Komanduri, 1995; Komanduri and Hou, 2002). Figure 15 shows the chip shape at high magnification, and highlights the shear planes. In general, chips are very small, almost powder-like, segmented, and with sharp edges, as a consequence of the low deformability that those alloys retain even at high temperatures.

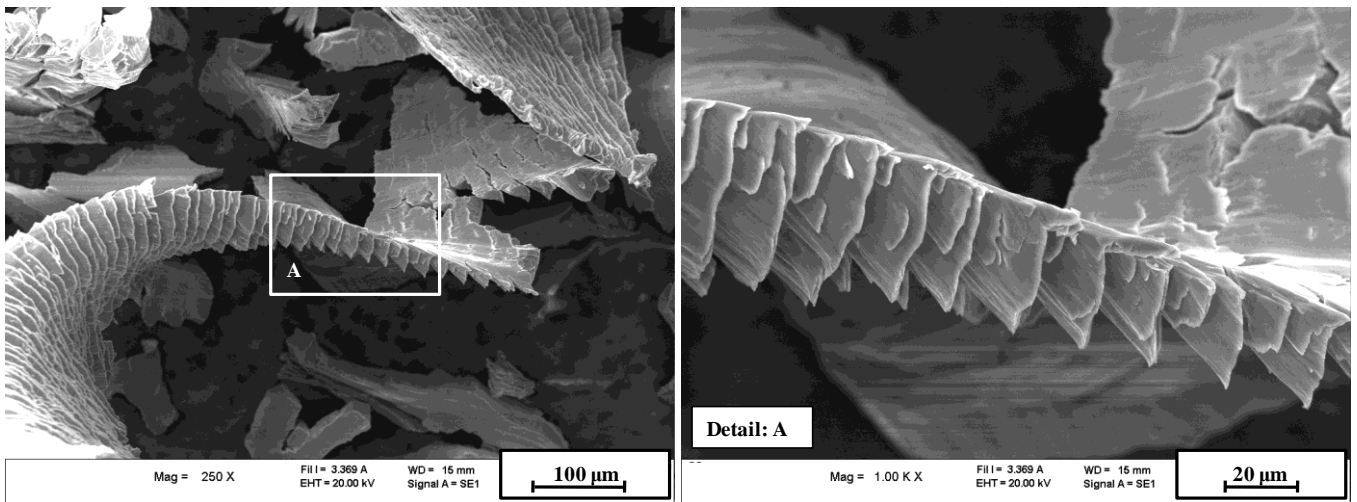


Figure 15: Chip morphology for an AlSiTiN coated mill subjected to a post-coating polishing treatment.

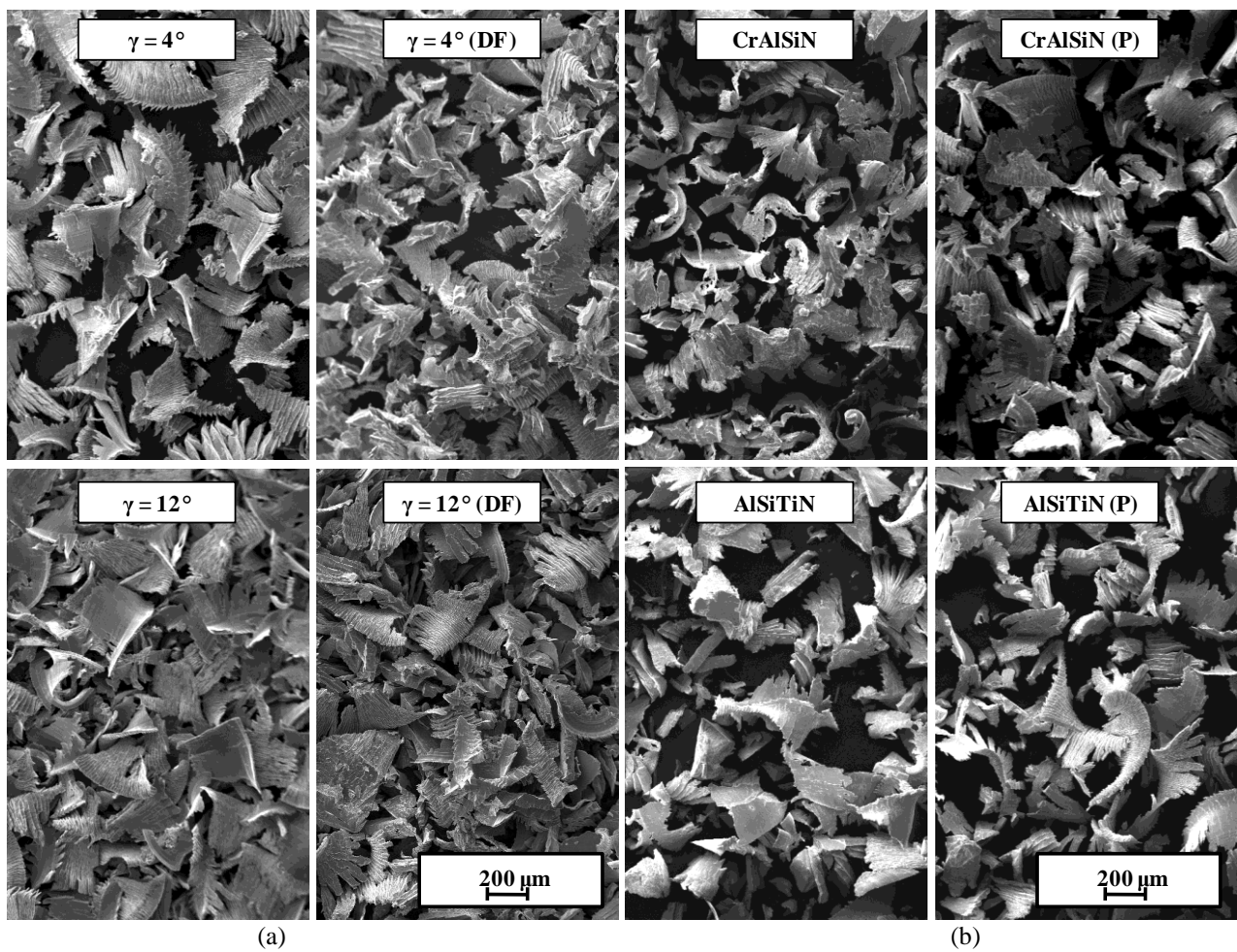


Figure 16: Chip morphology for uncoated (a) and coated (b) tools.

As far as the effects of the different cutting tool geometries/coatings is concerned, Figure 16 evidences that a perceivable modification in chip shape as a result of the drag finishing process is observed, both for uncoated and coated tools. In particular, the chips appears less regular, highly crumbled, shorter, and smaller. The reduction of the surface roughness of the

cutting tool edges decreases friction, leading to a lower temperature in the shear zone: as a consequence, the material is less deformable.

4. Conclusions

A strategy to improve machinability of an EBM sintered gamma titanium aluminide was presented, including an adjustment of cutting edge geometry. The results of the milling tests performed for a fixed cutting condition show that the reduction of radial rake angle from $\gamma = 12^\circ$ to $\gamma = 4^\circ$ yields a benefit in terms of tool life. Furthermore, the drag finishing process, by increasing the edge radius and improving the edge surface quality, also allows a reduction in tool wear.

The tests performed with nanogradient coatings highlight that tool life can be increased by using an appropriate coating system, and that AlSiTiN coating performs better than CrAlSiN coating. In addition, a further reduction of tool wear is obtained with polishing treatment after coating. For all the experimental tests the surface roughness was suitable to satisfy the restrictive requirements for parts in aircraft engines, and the best result was obtained by the mills with the AlSiTiN coating, subjected to the polishing post-treatment.

As far as surface hardness is concerned, the trends show that the milled surface hardness increases proportionally with tool wear, as a result of strain hardening. In addition, the drag finishing process as well as the polishing treatment after coating involve a moderate reduction of surface hardness, while the hardness of the surfaces milled with coated tools is higher than that obtained with uncoated mills.

Observations of the milled surfaces, with both coated and uncoated tools, showed the presence of micro-craters, due to the microstructure of the workpiece, which was produced from metal powders. Finally, chips produced by milling operations were of a shear-localized form, very small, almost powder-like, segmented, and with sharp edges. A modification in chip shape as a result of the drag finishing process was observed, both for uncoated and coated tools.

Acknowledgments

The authors would like to thank AvioProp for providing the EBM gamma-TiAl alloy, and gratefully acknowledge Elisa Aimo Boot and Federico Cartasegna of Environment Park S.P.A. for coatings development and deposition. Finally, the authors wish to thank the Piedmont Region for funding this research within the framework of the MANUNET project.

References

- Aspinwall, D.K., Dewes, R.C., Mantle, A.L., 2005. The machining of γ -TiAl intermetallic alloys. CIRP Annals - Manufacturing Technology 54 (1), 99-104.
- Beranoagirre, A., López de Lacalle, L.N., 2010. Optimizing the milling of titanium aluminide alloys. Int. J. Mechatronics and Manufacturing Systems 3 (5/6), 425-436.
- Cormier, D., Harrysson, O., Mahale, T., West, H., 2007. Freeform fabrication of titanium aluminide via electron beam melting using prealloyed and blended powders, Research Letters in Materials Science, Hindawi Publishing Corporation 1-4.
- Cotterell, M., Byrne, G., 2008. Dynamics of chip formation during orthogonal cutting of titanium alloy Ti-6Al-4V. Annals of the CIRP 57 (1), 93-96.
- Hou, Z.B., Komanduri, R., 1995. On a thermomechanical model of shear instability in machining. Annals of the CIRP 44 (1), 69-73.
- Klocke, F., Stegen, A., Fritsch, R., 2008. Grundlagenuntersuchungen zur ultraschallunterstützten Zerspanung intermetallischer gamma-Titanaluminidlegierungen, DFG Abschlussbericht.
- Komanduri, R., Hou, Z.B., 2002. On thermoplastic shear instability in the machining of a titanium alloy (Ti-6Al-4V), Metallurgical and materials transactions A 33 (9), 2995-3010.
- Liu, C.T., Maziasz, P.J., 1998. Microstructural control and mechanical properties of dual-phase TiAl alloys. Intermetallics 6 (7-8), 653-661.
- Liu, Z.C., Lin, J.P., Li, S.J., Cheng, G.L., 2002. Effects of Nb and Al on the microstructures and mechanical properties of high Nb containing TiAl base alloys. Intermetallics 10 (7), 653-659.
- Mantle, A.L., Aspinwall, D.K., 2001. Surface integrity of a high speed milled gamma titanium aluminide. Journal of Materials Processing Technology 118, 143-150.

Murr, L.E., Quinones, S.A., Gaytan, S.M., Lopez, M.I., Rodela, A., Martinez, E.Y., Hernandez, D.H., Martinez, E., Medina, F., R.B. Wicker, Microstructure and mechanical behavior of Ti-6Al-4V produced by rapid-layer manufacturing for biomedical applications, *Journal of the Mechanical Behavior of Biomedical Materials* 2 (1) (2009) 20-32.

Petropoulos, G.P., Pandazaras, C.N., Davim, J.C., West, H., 2010. Surface texture characterization and evaluation related to machining, Springer-Verlag, London Limited, UK.

Priarone, P.C., Rizzuti, S., Rotella, G., Settineri, L., 2011. Tool wear and surface quality in milling of a gamma-TiAl intermetallic, *International Journal of Advanced Manufacturing Technology* (doi:10.1007/s00170-011-3691-x).

Settineri, L., Faga, M.G., Gautier, G., Perucca, M., 2008. Evaluation of wear resistance of AlSiTiN and AlSiCrN nanocomposite coatings for cutting tools, *CIRP Annals, Manufacturing Technology* 57 575-578.

Yu, K.O., 2001. Modeling for casting & solidification processing, Series Materials Engineering, Taylor & Francis Group.

Figure captions

Figure 1: EBM sintered workpiece, as supplied.

Figure 2: Workpiece microstructure, at different magnifications: 50X (a) and 200X (b).

Figure 3: Workpiece grinded prior to milling operations.

Figure 4: Fresh tool geometry comparisons.

Figure 5: OTEC DF 70 drag finishing machine.

Figure 6: Structure of the experimental gradient coatings.

Figure 7: Tool wear observations. The images refer to an uncoated mill with radial rake angle $\gamma = 12^\circ$, without drag finishing treatment, and after 16 minutes of machining time.

Figure 8: SEM images of an AlSiTiN coated edge after 40 min of milling time: tool tip (a), secondary flank face (b), and rake face (c).

Figure 9: EDS analysis of adherent workpiece material.

Figure 10: Experimental tool wear curves, for uncoated (a) and coated tools (b).

Figure 11: Roughness results.

Figure 12: Surface hardness results for uncoated tools with radial rake angle $\gamma = 12^\circ$ (a) and $\gamma = 4^\circ$ (b).

Figure 13: Surface hardness results for CrAlSiN (a) and AlSiTiN (b) nanocoated tools. Tool geometry is $\gamma = 4^\circ$ and $r_\beta \approx 15 \mu\text{m}$.

Figure 14: Micrograph of the milled surface (500X) for different coated tools.

Figure 15: Chip morphology for an AlSiTiN coated mill subjected to a post-coating polishing treatment.

Figure 16: Chip morphology for uncoated (a) and coated (b) tools.

Table captions

Table 1: Chemical composition of EBM sintered γ -TiAl alloy.

Table 2: End mills geometrical parameters.

Table 3: Uncoated tools for cutting tests.

Table 4: Coated tools for cutting tests.

Effects of cutting angle, edge preparation, and nano-structured coating on milling performance of a gamma titanium aluminide

Figures



Figure 1: EBM sintered workpiece, as supplied

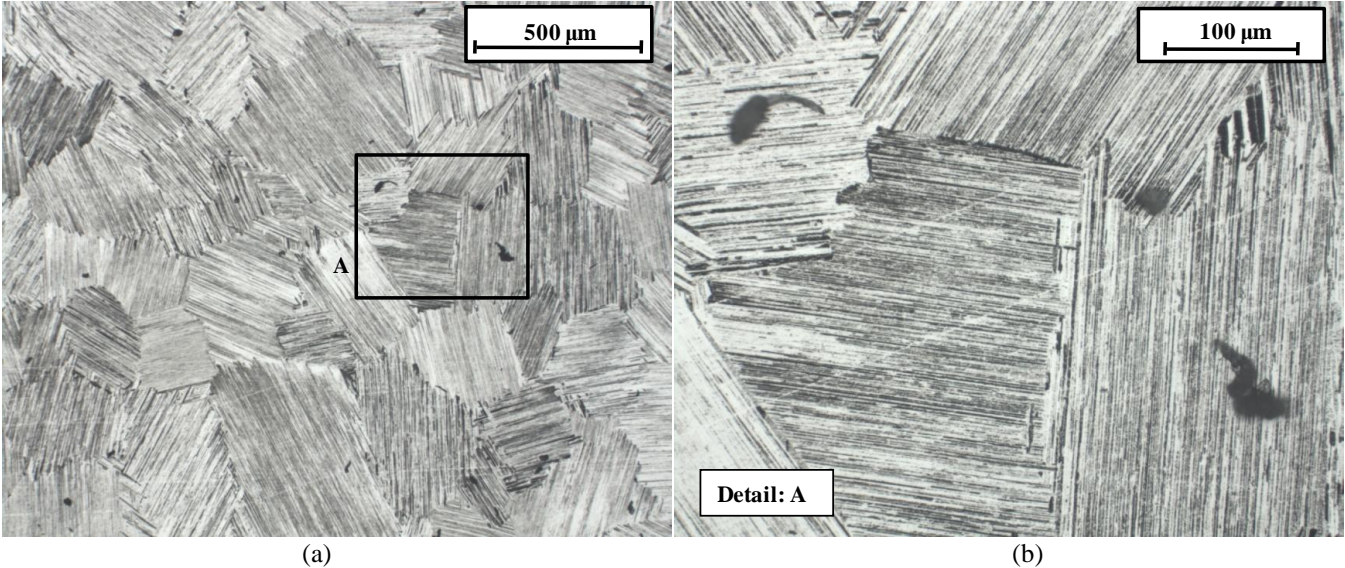


Figure 2: Workpiece microstructure, at different magnifications: 50X (a) and 200X (b).

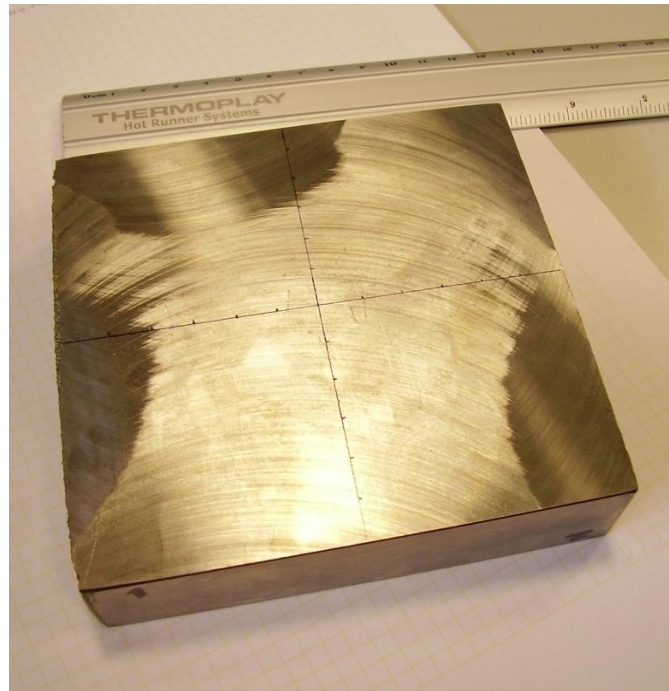


Figure 3: Workpiece grinded prior to milling operations

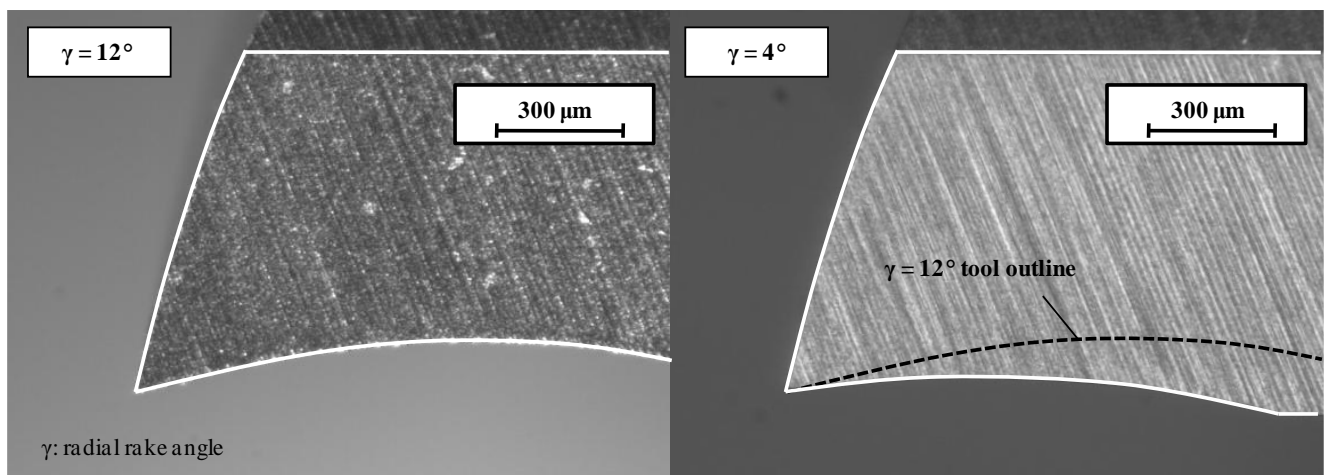


Figure 4: Fresh tool geometry comparisons



Figure 5: OTEC DF 70 drag finishing machine

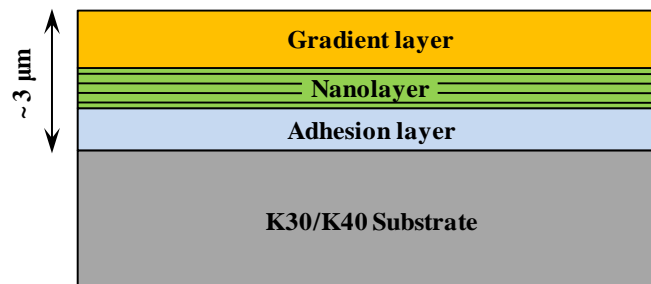


Figure 6: Structure of the experimental gradient coatings

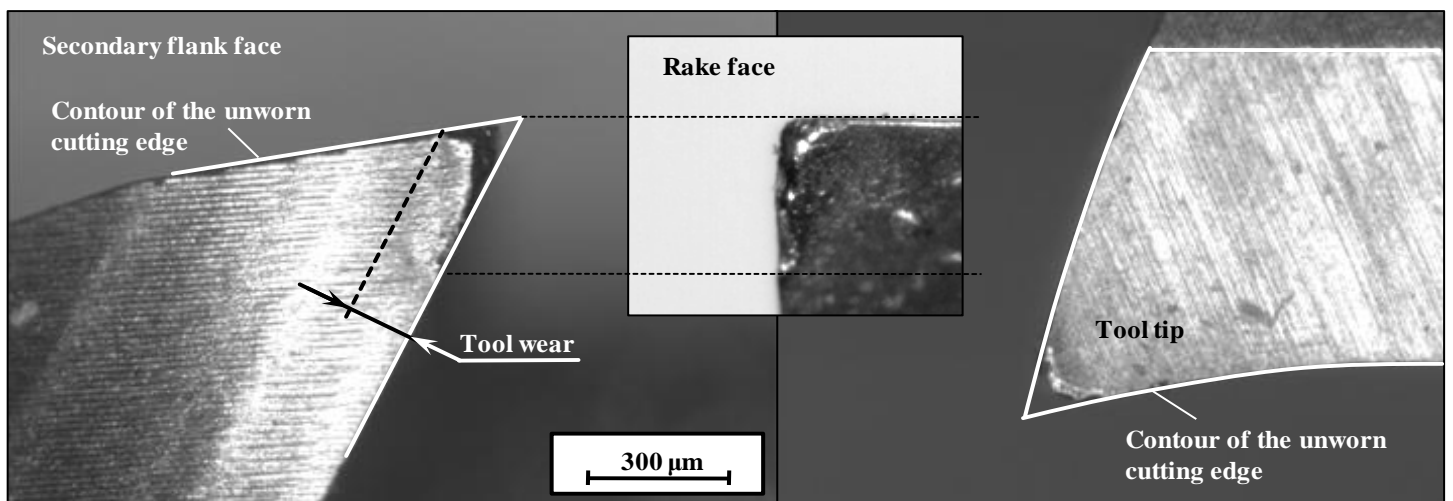
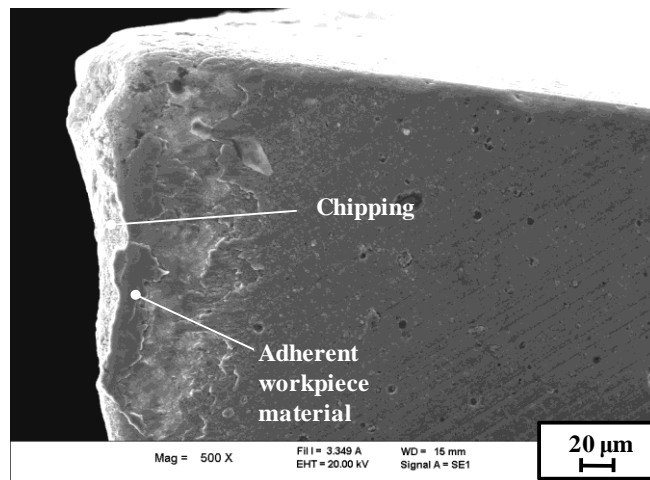
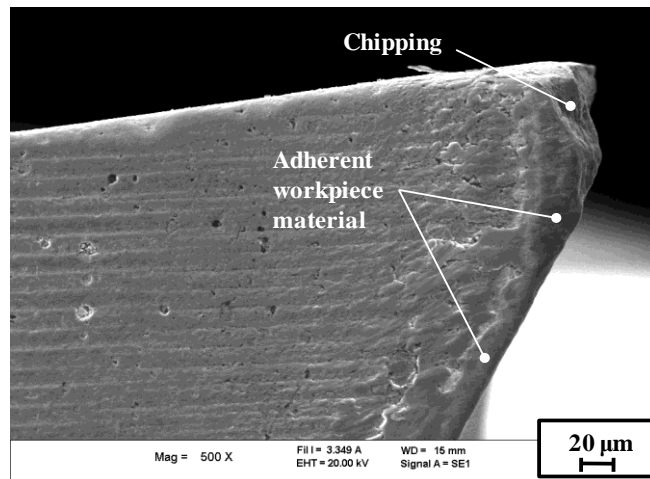


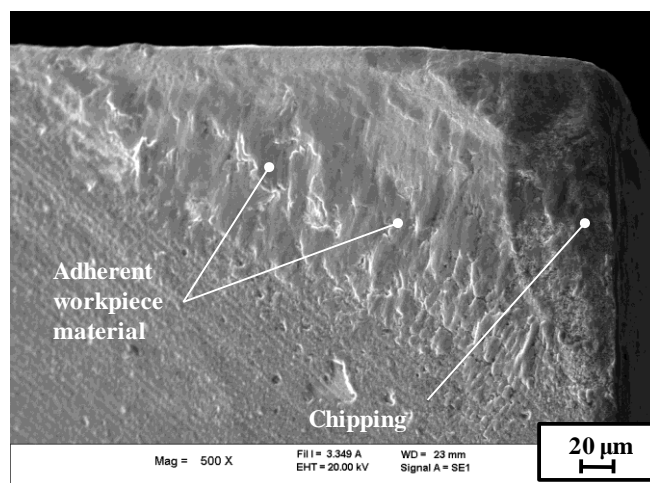
Figure 7: Tool wear observations. The images refer to an uncoated mill with radial rake angle $\gamma = 12^\circ$, without drag finishing treatment, and after 16 minutes of machining time.



(a)



(b)



(c)

Figure 8: SEM images of an AlSiTiN coated edge after 40 min of milling time: tool tip (a), secondary flank face (b), and rake face (c)

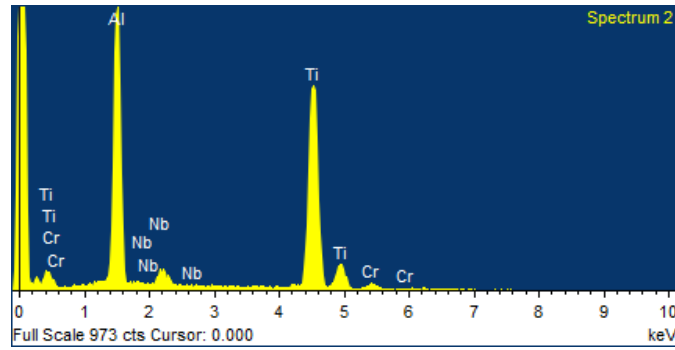


Figure 9: EDS analysis of adherent workpiece material

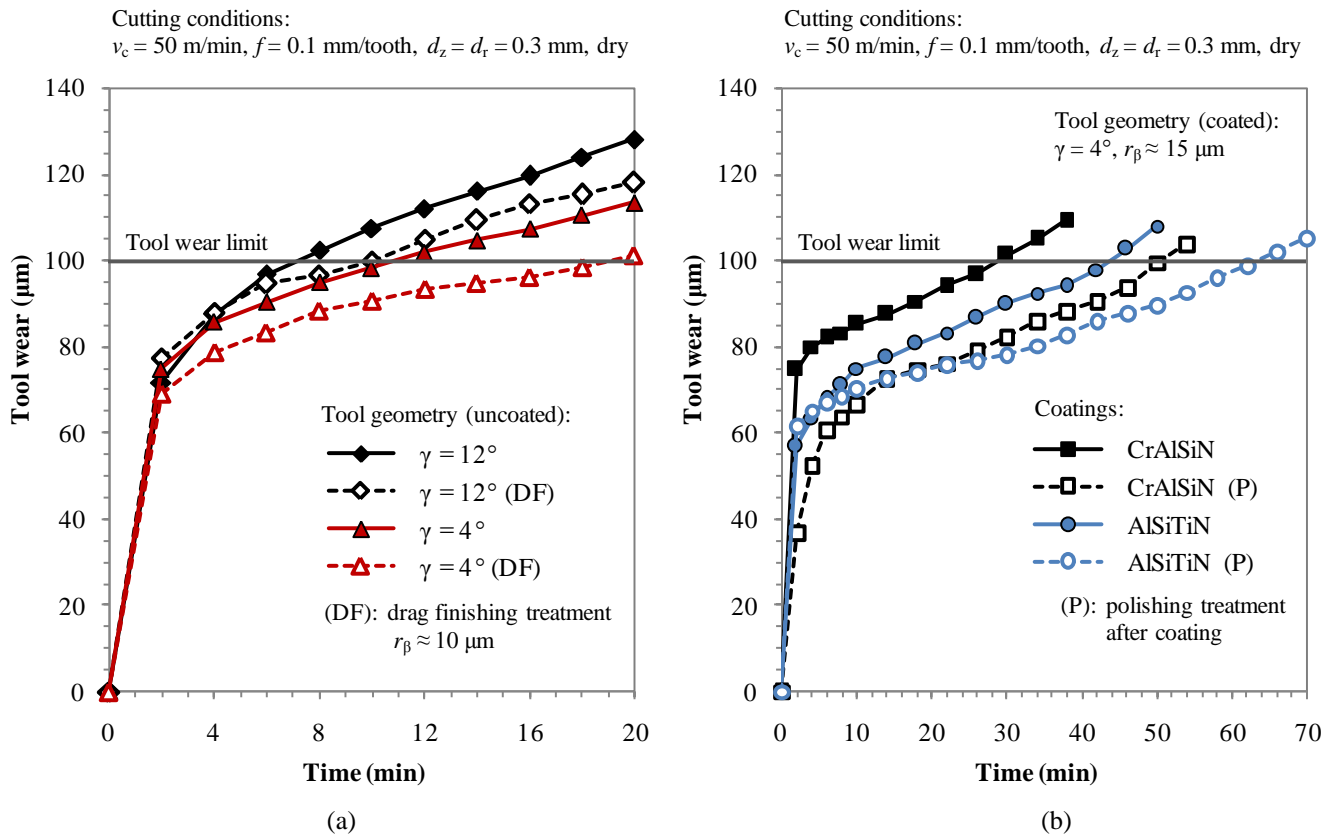


Figure 10: Experimental tool wear curves, for uncoated (a) and coated tools (b).

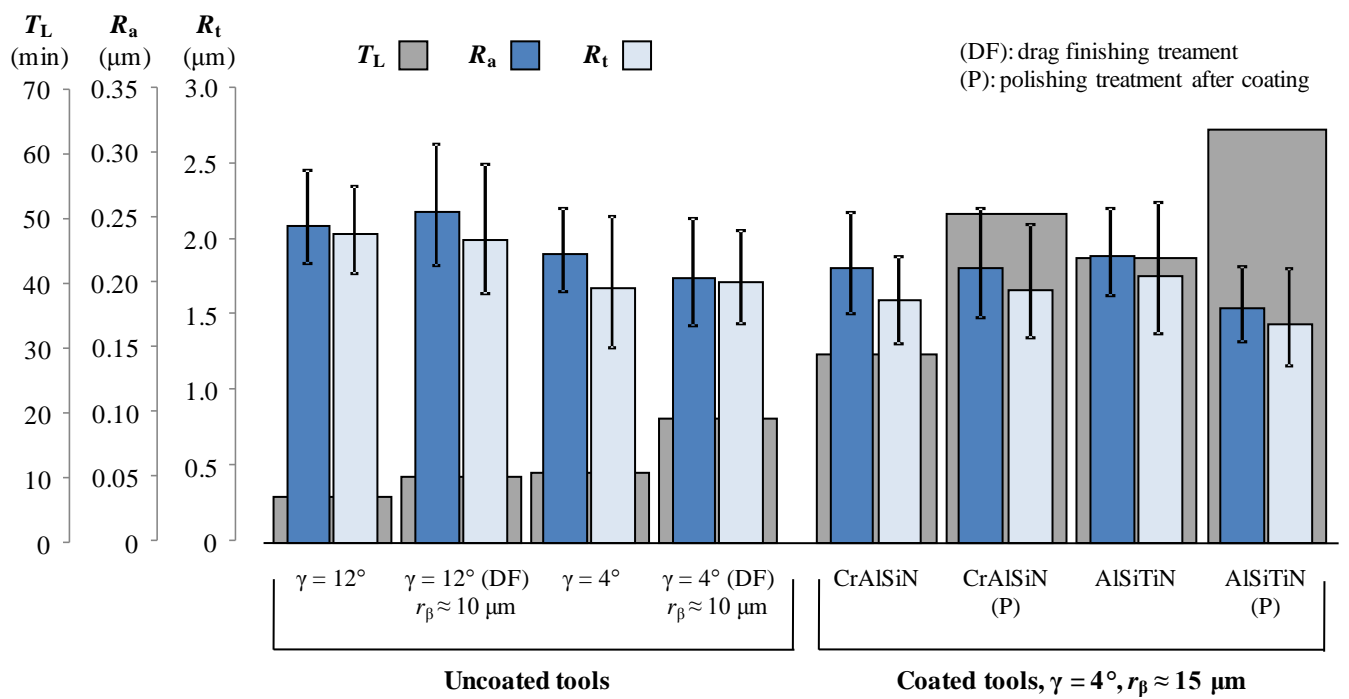
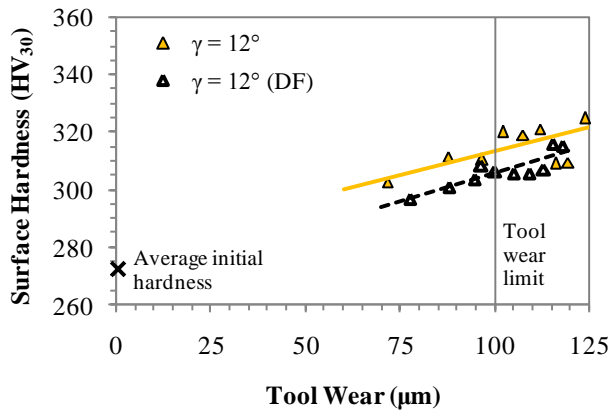
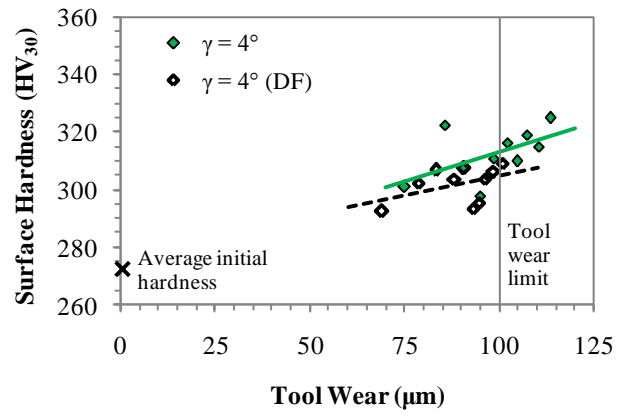


Figure 11: Roughness results.

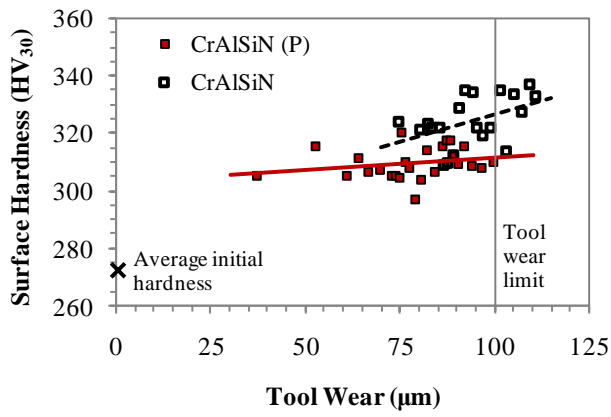


(a)

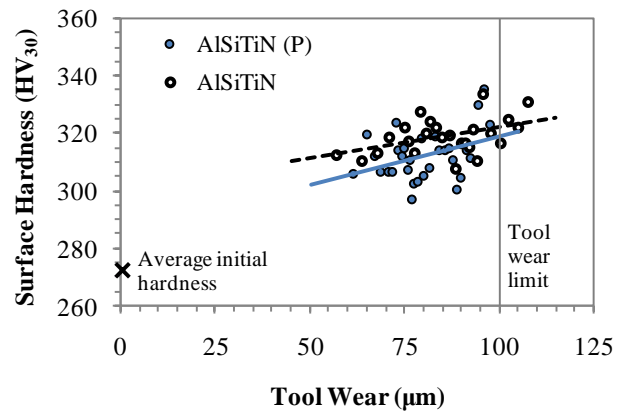


(b)

Figure 12: Surface hardness results for uncoated tools with radial rake angle $\gamma = 12^\circ$ (a) and $\gamma = 4^\circ$ (b).



(a)



(b)

Figure 13: Surface hardness results for CrAlSiN (a) and AlSiTiN (b) nanocoated tools. Tool geometry is $\gamma = 4^\circ$ and $r_\beta \approx 15 \mu\text{m}$.

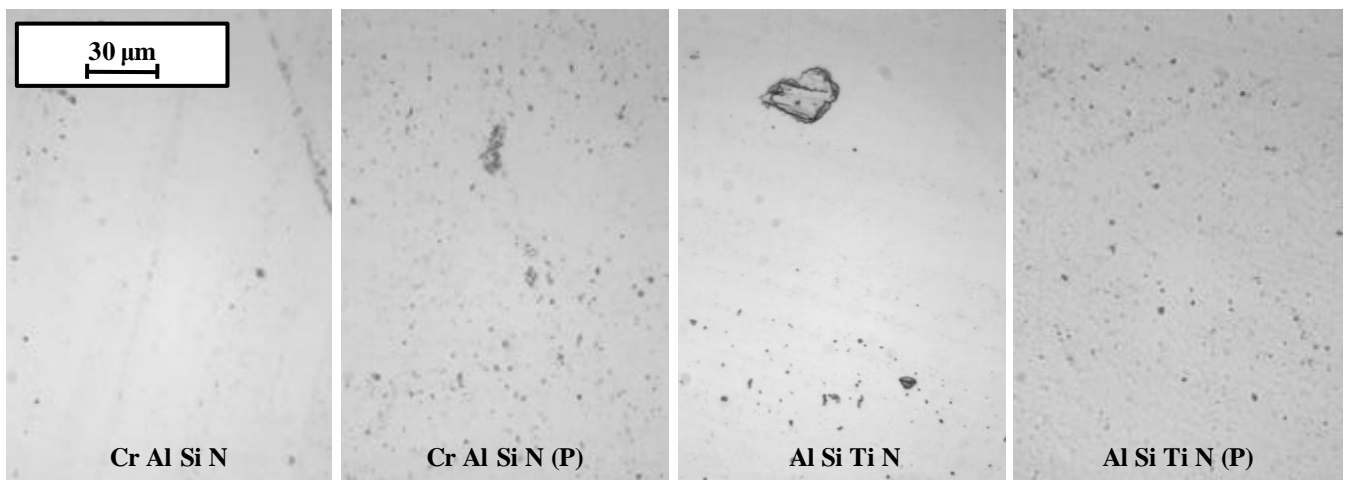


Figure 14: Micrograph of the milled surface (500X) for different coated tools.

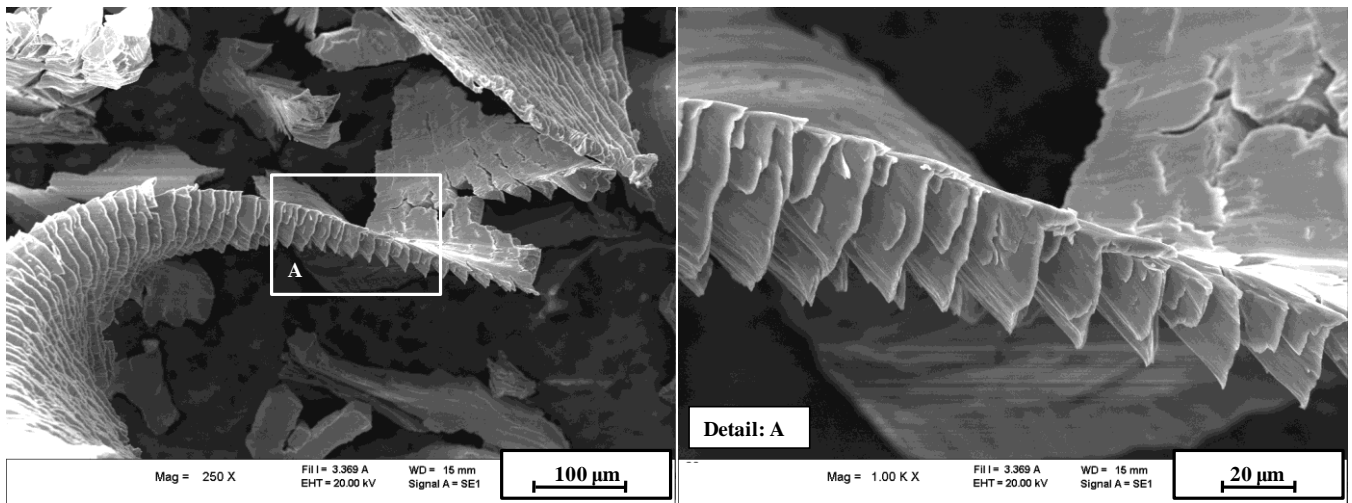


Figure 15: Chip morphology for an AlSiTiN coated mill subjected to a post-coating polishing treatment.

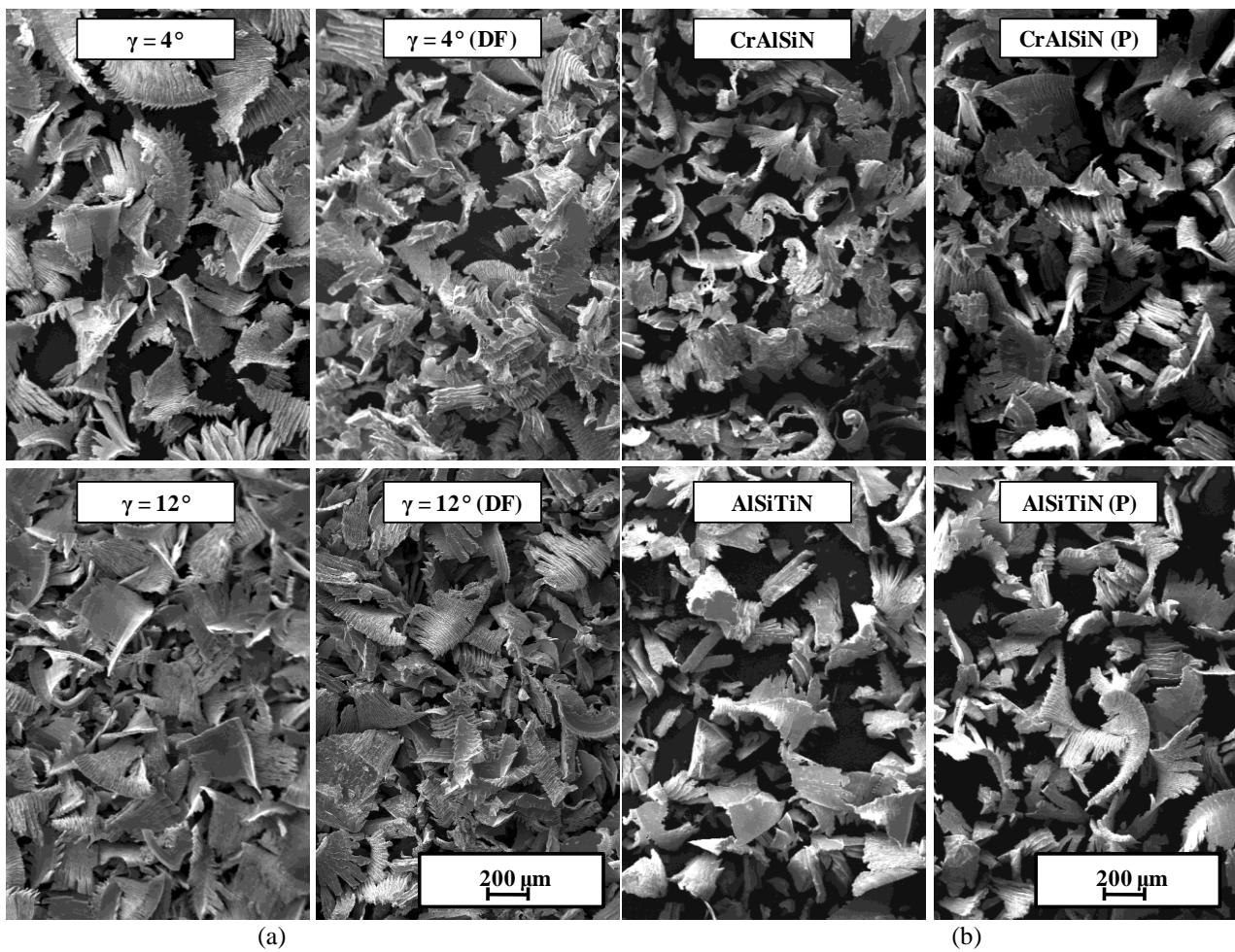


Figure 16: Chip morphology for uncoated (a) and coated (b) tools.

Effects of cutting angle, edge preparation, and nano-structured coating on milling performance of a gamma titanium aluminide

Tables

Element	Weight percent
Aluminum	32.0 - 33.5
Niobium	4.5 - 5.1
Chromium	2.2 - 2.6
Oxygen	Max 0.08
Nitrogen	Max 0.02
Carbon	Max 0.015
Iron	Max 0.04
Hydrogen	Max 0.001
All others	Max 0.05
Titanium	Balance (Max 60%)

Table 1: Chemical composition of EBM sintered γ -TiAl alloy.

Parameter	Value
Mill diameter (mm)	10
Shank diameter (mm)	10
Length of cut (mm)	23
Overall length (mm)	72
Axial rake angle ($^{\circ}$)	4
Axial primary relief angle ($^{\circ}$)	6
Axial secondary clearance angle ($^{\circ}$)	16
End cutting edge concavity angle ($^{\circ}$)	2
Helix angle ($^{\circ}$)	30
Radial rake angle ($^{\circ}$)	12; 4
Radial primary relief angle ($^{\circ}$)	12
Radial secondary clearance angle ($^{\circ}$)	12

Table 2: End mills geometrical parameters

Test	Radial rake angle $\gamma(^{\circ})$	Edge treatment	Radius of edge roundness $r_{\beta}(\mu\text{m})$	Average edge roughness $R_{a\beta}(\mu\text{m})$
1	12	None	≈ 5	0.64
2	12	Drag finishing	≈ 10	0.49
3	4	None	≈ 5	0.40
4	4	Drag finishing	≈ 10	0.23

Table 3: Uncoated tools for cutting tests

Test	Radial rake angle $\gamma(^{\circ})$	Edge pre-treatment (before coating)	Radius of edge roundness $r_{\beta}(\mu\text{m})$	Average edge roughness $R_{a\beta}(\mu\text{m})$	Coating	Edge post-treatment (after coating)
5	4	Drag finishing	≈ 15	0.20	AlSiTiN	None
6					AlSiTiN	Polishing
7					CrAlSiN	None
8					CrAlSiN	Polishing

Table 4: Coated tools for cutting tests